

Comparison of Pulsed and Pseudocontinuous Arterial Spin-Labeling for Measuring CO₂-Induced Cerebrovascular Reactivity

Felipe B. Tancredi, BEng,^{1,2*} Claudine J. Gauthier, MSc,^{2,3} Cécile Madjar, MSc,² Divya S. Bolar, PhD,^{4–6} Joseph A. Fisher, MD,⁷ Danny J.J. Wang, PhD,⁸ and Richard D. Hoge, PhD^{1–3}

Purpose: To compare the performance of pulsed and pseudocontinuous arterial spin-labeling (PASL and pCASL) methods in measuring CO₂-induced cerebrovascular reactivity (CVR).

Materials and Methods: Subjects were scanned using both ASL sequences during a controlled hypercapnia procedure and visual stimulation. CVR was computed as the percent CO₂-induced increase in cerebral blood flow ($\Delta\%$ CBF) per mmHg increase in end-tidal PCO₂. Visually evoked responses were expressed as $\Delta\%$ CBF. Resting CBF and temporal signal-to-noise ratio were also computed. Regionally averaged values for the different quantities were compared in gray matter (GM) and visual cortex (VC) using *t*-tests.

Results: Both PASL and pCASL yielded comparable respective values for resting CBF (56 ± 3 and 56 ± 4 mL/min/100g) and visually evoked responses ($75 \pm 5\%$ and $81 \pm 4\%$). Values of CVR determined using pCASL (GM

4.4 ± 0.2 , VC 8 ± 1 $\Delta\%$ CBF/mmHg), however, were significantly higher than those measured using PASL (GM 3.0 ± 0.6 , VC 5 ± 1 $\Delta\%$ CBF/mmHg) in both GM and VC. The percentage of GM voxels in which statistically significant hypercapnia responses were detected was also higher for pCASL ($27 \pm 5\%$ vs. $16 \pm 3\%$ for PASL).

Conclusion: pCASL may be less prone to underestimation of CO₂-induced flow changes due to improved label timing control.

Key Words: ASL; hypercapnia; cerebrovascular reactivity
J. Magn. Reson. Imaging 2012;000:000–000.
 © 2012 Wiley Periodicals, Inc.

HYPERCAPNIA is known to elicit a global increase in cerebral blood flow (CBF) (1,2), a phenomenon that has been exploited in various magnetic resonance imaging (MRI) applications including measures of cerebrovascular reactivity (CVR) (3,4) and calibrated MRI for estimation of task-induced cerebral metabolic rate of oxygen (CMRO₂) changes (5,6). These techniques rely on arterial spin-labeling (ASL), which provides dynamic and noninvasive images of CBF.

Pulsed ASL (PASL) has long been the predominant form of ASL, due possibly to simpler implementation and broader compatibility with available MRI hardware. The continuous approach (CASL), which was the earliest ASL method proposed (7), offers several theoretical advantages but its adoption has been limited due to the complexity of controlling for off-resonance effects in multislice scans and the high transmitted radiofrequency (RF) power demanded. The recent introduction of pseudocontinuous ASL (pCASL) methods, which emulate the continuous irradiation with concatenated series of short RF pulses (8), has allowed the more widespread adoption of the CASL approach.

A major factor affecting the amplitude of the ASL subtraction signal is the dynamics of label timing (9–11). In PASL, techniques such as QUIPSS I and II (12), and variants such as Q2TIPS (13), have been adopted to impose a fixed duration to the label

¹Institut de génie biomédical, Département de physiologie, Université de Montréal, Montreal, Quebec, Canada.

²Unité de neuroimagerie fonctionnelle, Centre de recherche de l'institut universitaire de gériatrie de Montréal, Montreal, Quebec, Canada.

³Département de physiologie, Faculté de médecine, Université de Montréal, Montreal, Quebec, Canada.

⁴Athinoula A. Martinos Center for Biomedical Imaging, Massachusetts General Hospital, Charlestown, Massachusetts, USA.

⁵Harvard-MIT Division of Health Sciences and Technology, Harvard Medical School, Massachusetts Institute of Technology, Cambridge, Massachusetts, USA.

⁶Department of Electrical Engineering and Computer Science, Massachusetts Institute of Technology, Cambridge, Massachusetts USA.

⁷Department of Anesthesiology, University Health Network, University of Toronto, Toronto, Canada.

⁸University of California Los Angeles, Los Angeles, California, USA.

Contract grant sponsor: Canadian Institutes for Health Research; Contract grant number: MOP 84378 (Banting and Best Scholarship held by C.J.G.); Contract grant sponsor: Canadian Foundation for Innovation; Contract grant number: Leaders Opportunity Fund 17380; Contract grant sponsor: Ministère du développement économique, de l'innovation et de l'exportation; Contract grant number: PSR-SIIRI-239.

*Address reprint requests to: F.B.T., 4545 Queen Mary, M6808, Montreal, QC, Canada, H3W 1W5. E-mail: felipe.tancredi@umontreal.ca

Received February 21, 2011; Accepted March 7, 2012.

DOI 10.1002/jmri.23658

View this article online at wileyonlinelibrary.com.

passage and hence avoid inaccuracies associated with changes in the latter parameter. Label duration is controlled as long as the trailing edge of the tagged blood bolus does not exit the initial tagging region before the saturating pulses are applied. During global flow increases, which are known to have a large impact on the flow velocity in the major arteries feeding the brain (14), it is possible that the trailing edge of the label bolus will clear the tag region earlier, rendering QUIPSS saturation pulses ineffective and creating a situation that underestimates flow.

A potential advantage of CASL (and variants such as pCASL) for quantification of flow changes during hypercapnia is that it provides an implicit control over the label duration. CASL also offers an inherently higher flow contrast, resulting in increased temporal signal-to-noise ratio (SNR) of individual flow subtraction images, albeit at the expense of a slightly lower imaging rate (reducing statistical power). The longer minimum TR value typically associated with CASL techniques is less of a limitation for hypercapnic manipulations, which tend to use relatively long block designs. A potential confound is that CASL's labeling efficiency may be altered by changes in the arterial flow velocity (15–17).

A number of recent studies have compared the sensitivity and quantitative results provided by PASL and CASL for both baseline flow and the local responses observed in neuronal activation paradigms (8,17–19), but there has been no systematic comparison of the performance of these two types of ASL during hypercapnic manipulations, and in fact very few hypercapnia studies to date have used CASL.

The aim of this study was to compare the performance of two ASL sequences in measuring global CBF responses elicited by mild hypercapnia: one using the widely adopted PICORE Q2TIPS pulsed labeling approach, and one using pseudocontinuous labeling. The local flow responses stimulated by a visual paradigm were also examined.

MATERIALS AND METHODS

Ten healthy subjects were recruited for the study (two females, eight males, ages 24–33). All subjects gave informed consent and the protocol was approved by the Research Ethics Committee of our institution.

Functional MRI Protocol

Each functional imaging run consisted of three blocks of baseline alternated with two blocks of stimulation, each lasting 120 seconds. In two runs the manipulation consisted of a step increase in end-tidal PCO_2 (P_{ETCO_2}), while in the other two runs a visual stimulus was used. The order of the conditions was randomly varied between subjects.

Visual Stimulation

The visual stimulus was a black-and-white radial checkerboard, contrast reversing at 16 Hz. The stimu-

lus was presented using an LCD projector (EMP-8300, Epson, Toronto, ON, Canada) onto a translucent screen viewed by subjects through a mirror integrated into the Siemens head coil. The visual baseline was a uniform gray screen with the same spatial mean luminance as the checkerboard pattern. Subjects breathed atmospheric composition medical air throughout visual stimulation runs.

Hypercapnic Manipulation

P_{ETCO_2} and end-tidal PO_2 (P_{ETO_2}) were independently targeted via the administration of gases containing mixtures of O_2 , CO_2 , and N_2 to a sequential gas-delivery breathing circuit (20) by a computer-controlled gas blender (21) (RespirAct, Thornhill Research, Toronto, ON, Canada). The RespirAct was programmed to maintain a constant P_{ETCO_2} of 40 mmHg and P_{ETO_2} at 100 mmHg at baseline, and iso-oxic (P_{ETO_2} maintained at 100 mmHg) increase in P_{ETCO_2} by 5 mmHg for the hypercapnic stimulus. P_{ETCO_2} and P_{ETO_2} were monitored continuously by the RespirAct and as a safety measure pulse rate and arterial O_2 saturation were also monitored using a pulse-oximeter (InVivo Instruments, Orlando, FL).

The same gray screen and fixation marker used as the baseline condition in the visual stimulation protocol was maintained throughout the hypercapnia runs.

MRI Acquisition

Imaging was performed on a 3 T scanner (TIM Trio, Siemens Medical Solutions, Erlangen, Germany) using a 32-channel receive-only head coil. A T1-weighted anatomical acquisition (MPRAGE with $\text{TR}/\text{TE}/\alpha = 2300/3 \text{ msec}/90^\circ$ 256×240 matrix and 1 mm^3 resolution) was followed by four functional scanning runs.

Each of the stimulation paradigms (hypercapnia and visual) were carried out with both types of ASL scan (PASL and pCASL). Pulsed ASL was performed using the PICORE labeling geometry (22) with a tag width of 160 mm and a 10 mm gap. The Q2TIPS method (13) was used with $\text{TI}_1/\text{TI}_2 = 700/1400 \text{ msec}$ and stop time 1350 msec. Other sequence parameters were $\text{TR}/\text{TE}/\alpha = 2000/10 \text{ msec}/90^\circ$.

In the pCASL acquisitions, labeling was performed over a 1.5-second period using a series of 25° Hanning window-shaped RF pulses of 500 μs duration and separated by 360- μs gaps. These were applied along with a 6 mT/m gradient to place the labeling plane 100 mm below the center of the imaged volume. A postlabeling delay of 900 msec was used, while other sequence parameters were $\text{TR}/\text{TE}/\alpha = 3000/10 \text{ msec}/90^\circ$.

For both types of ASL the same gradient-echo EPI with fat saturation was used (slices 6 mm thick, 1 mm gap, 4 mm in-plane resolution, 64×64 matrix and bandwidth of 3 kHz/pixel), using a partial k -space acquisition factor of 7/8 and GRAPPA parallel imaging (acceleration factor of two (23)). In the PASL scans six slices were acquired, while 16 slices were imaged in the pCASL acquisitions. The different numbers of slices were due to implementation details of

the respective ASL sequences; care was taken in subsequent analyses to control for this. The stack of oblique axial slices were positioned to maximize coverage of the occipital lobe and oriented along a plane passing through the trunk and splenium of the corpus callosum.

Image Analysis

All MRI data were analyzed using the Neurolens software package (www.neurolens.org). Image series were first motion-corrected (24), spatially smoothed (6 mm full-width at half-maximum [FWHM] 3D Gaussian kernel), and intensity normalized. The flow-weighted signal was then isolated using linear surround subtraction. Voxel-wise CBF response amplitudes for each condition (visual stimulation or hypercapnia, henceforth referred to as “visual” or “CO₂” conditions) were then estimated by fitting the time-course data with a general linear model (GLM) consisting of a block response term (convolved with a single-gamma hemodynamic response function: HRF time-to-peak = 5.4 sec, FWHM = 5.2 sec) (25) plus a third-order polynomial to model resting flow and drift. Global CBF responses to hypercapnia were estimated by defining a gray matter (GM) region of interest (ROI) mask for each subject. These ROIs were generated through segmentation of the MPRAGE acquisition and resampled to the spatial resolution of the ASL scans.

To estimate CBF responses in visual cortex (VC) evoked by the visual and hypercapnic stimuli, ROIs were defined based on activation maps for the visual stimulation data (circular bias was avoided through steps described below). For both ASL types a VC ROI was first derived from the visual activation map by thresholding the T-maps at $P < 0.001$ and manually removing activated regions outside the occipital lobe. Visual stimulation responses achieved very high significance in most subjects with both techniques, permitting a more stringent threshold P value (0.001) than was later used to assess the detection power for hypercapnic responses ($P \leq 0.05$). The large visual response meant that the statistical detection of visual responses was substantially “overpowered,” making the visual ROI largely insensitive to the exact threshold used (mitigating concerns about potential circularity in this approach).

The threshold T-values were determined as described (26), which takes into account the brain volume imaged and effective spatial resolution to correct for multiple comparisons. This resulted in slightly different threshold values for different subjects and scan techniques, but these were all very close to an average threshold value of 5.6. To remove the impact of total volume coverage on thresholding, this average threshold value was used in all 18 functional scans.

Since VC masks based on activation masks from a specific technique (referred to as “technique-specific VC”) are likely to emphasize voxels with large responses in the respective method, we also generated VC masks that were the union, or intersection, of the technique-specific VCs (referred to as union and intersection VC ROIs, respectively). Technique-specific VC

ROIs were utilized to compare the results that would be obtained in studies based entirely on one of the two ASL types. To rule out possible bias from ROI differences, we also performed comparisons using common VC ROIs, ie, the union or intersection VC ROIs.

To determine response amplitudes during visual stimulation and hypercapnia, the average GLM “effect-size” (based on the fit parameters, or β 's) within the ROI was used as the response amplitude, which was then divided by the ROI-averaged baseline (constant) term from the same model fit (β_0) and multiplied by 100 to convert to percent change. ROI-averaged time series were similarly expressed in percent change by normalizing the signal to the constant fit term after removing drift terms from the GLM fit.

We computed the mean $P_{ET}CO_2$ values for the different conditions (normocapnia and hypercapnia) and the true $P_{ET}CO_2$ increase as the difference between them (transition phases were excluded). The ROI-averaged CVR was computed by dividing the average percent change in CBF within the ROI by the $P_{ET}CO_2$ increase in mmHg.

We also computed the ROI-averaged temporal SNR (tSNR) for baseline flow and T-values for both baseline flow and functional responses from the model fit. The number of voxels for which the T-value exceeded a threshold corresponding to $P \leq 0.05$ was also determined for the different conditions. The tSNR was defined as the baseline CBF signal amplitude (from the constant term of the GLM model fit), divided by the root-mean-square value of the residual error between the measured signal at each voxel and the modeled signal. The use of GLM residuals, as opposed to simple mean and standard deviation values, provides stability measures, which we feel are more closely linked to statistical detection power.

A T-value for the estimate of baseline CBF was also computed (ie, testing the hypothesis that resting CBF was different from zero) as the constant term of the GLM model fit divided by the residual standard error (equivalent to the residual standard deviation adjusted for the number of images, and hence degrees of freedom, in the series). Similarly, T-values were computed for the response amplitudes during visual stimulation and hypercapnia. As a metric of the sensitivity of the two ASL methods for detection of resting flow and visual or hypercapnic responses, we first determined the number of voxels for which the T-value for the condition in question exceeded a threshold corresponding to $P \leq 0.05$ (corrected). The number of detected voxels was then divided by the total number of voxels in a given ROI (either GM or VC).

Maps of absolute flow—baseline and response to hypercapnia—were also generated using Eq. 1 in Ref. (27) for PASL and Eq. 1 in Ref. (28) for pCASL. For PASL, the following parameter values were used: blood-brain partition coefficient = 0.9, labeling efficiency = 0.95, blood T1 = 1.49 seconds, GM T1 = 1.4 seconds. The same parameters were used for pCASL, except that a labeling efficiency of 0.80 (8) was assumed. Baseline values were subsequently averaged within GM.

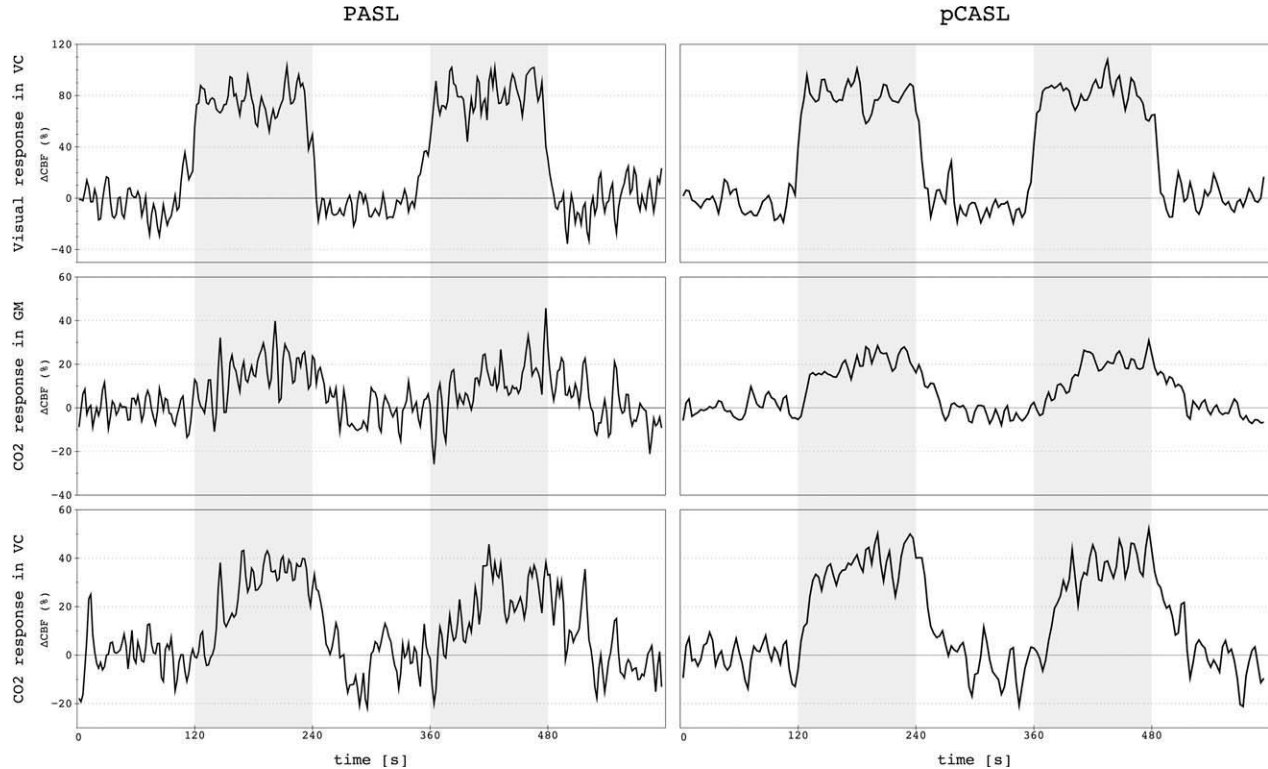


Figure 1. ASL signal time courses. Evoked CBF response signals for PASL (left) and pCASL (right) during visual stimulation and hypercapnia. ROI average signals are shown for hypercapnia in ROIs throughout all GM and also restricted to VC. Shaded regions in the plots indicate the 2-minute blocks of stimulation.

As the final analysis step, group averages were computed for percent effect-sizes, the ASL time series, CVR, tSNR, T-value, absolute baseline flow, and detection rate. Results are always shown as the group mean \pm standard error (SE).

Based on the above averages, we tested the hypothesis that PASL estimates of CVR are systematically lower than those obtained using pCASL by comparing measures from the respective techniques in a one-tailed Student's *t*-test. tSNR, T-values, and voxel counting were also compared using a one-tailed *t*-test. The resting flow values from the two methods were compared using a two-tailed *t*-test.

For qualitative comparisons, unthresholded maps of absolute CBF, tSNR, and various response measures such as effect-size, T-value, and Δ CBF were overlaid on high-resolution anatomic T1 scans. Unthresholded maps were used because this provided the truest depiction of sensitivity and specificity in the data (thresholding can introduce an “iceberg effect,” in which slightly subthreshold peaks or regions are obscured).

RESULTS

Data from one subject could not be used due to excessive artifacts in one of the PASL series.

Functional Response Signals

Figure 1 shows ROI average time courses recorded using the two ASL methods during visual stimulation and hypercapnia. For hypercapnia, signals are shown

for both GM and VC ROIs. It is qualitatively evident that the pCASL signals exhibit consistently better stability. Both techniques yield clearly discernible visual responses.

Baseline and CO₂ Response Maps

Both PASL and pCASL maps of baseline blood flow, shown in rows 2 and 3 of Fig. 2, provided a clear delineation of cortical anatomy—comparable to segmented GM masks shown in top row of the same figure—revealing the expected perfusion contrast between gray and white matter. Baseline CBF values measured in GM were 56 ± 3 and 56 ± 4 mL/min/100g for PASL and pCASL, respectively. Maps of the baseline tSNR (4th and 5th rows) were computed by dividing the baseline blood flow signal (ie, the effect size from the contrast selecting for the constant term in the linear model) by the residual standard deviation. The tSNR of PASL in GM was generally lower and more heterogeneous than that of pCASL. The bottom two rows of Fig. 2 show maps of the T-value for the resting flow signal, in which the baseline effect was divided by the residual standard error (taking into account the different imaging rates) instead of the standard deviation. This indicates that the improved per-image tSNR of pCASL and higher imaging rate of PASL balance each other (16), resulting in roughly equivalent overall statistical power for detection of baseline flow in both cases.

T-maps computed for the response to hypercapnia (Fig. 3, rows 1 and 2) generally exhibited large variations in sensitivity over cortical GM for both

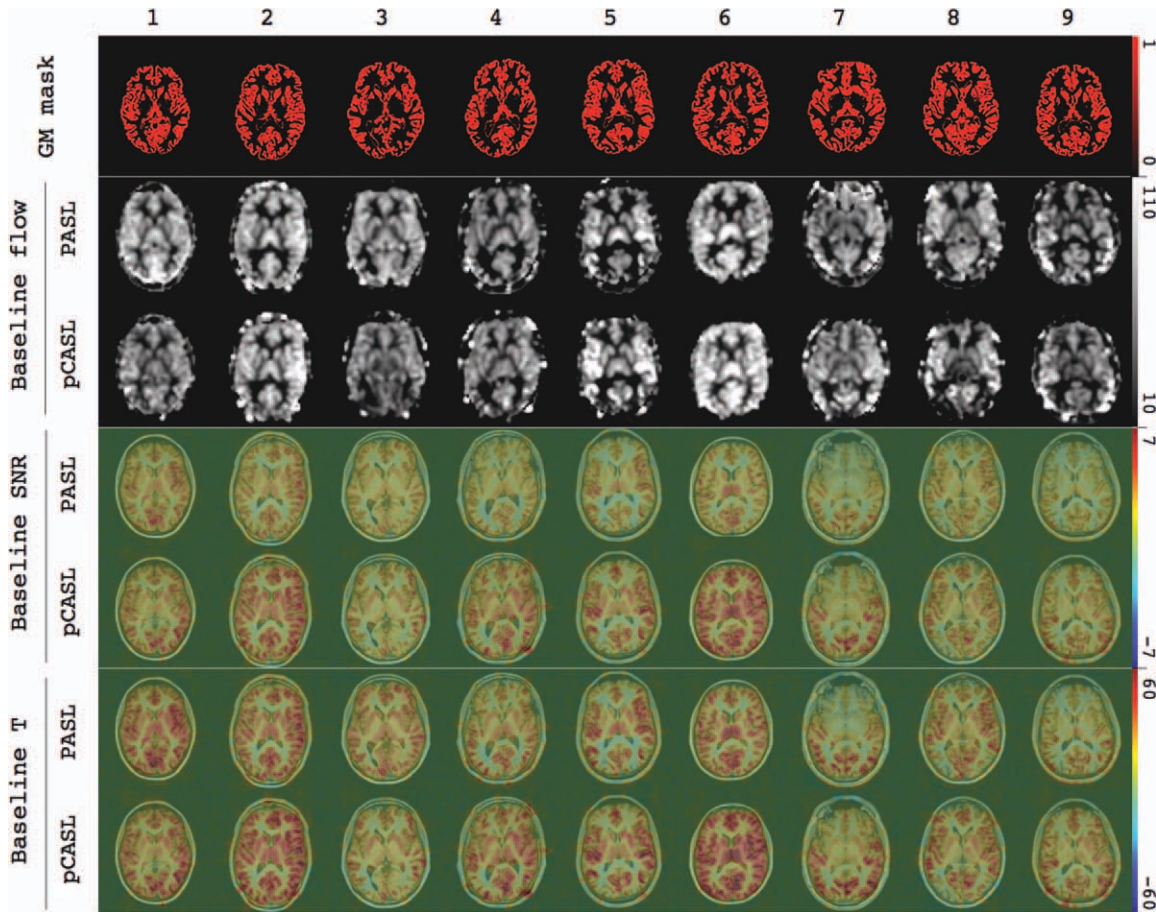


Figure 2. GM masks and baseline flow maps. The top row shows automatically segmented GM masks (red color scale) for all subjects. Subsequent rows show baseline flow maps, at the corresponding locations, acquired using PASL and pCASL (in alternating rows). Rows two and three show maps of absolute flow in units of mL/min/100g. Rows four and five show the SNR (β_0 divided by the GLM residual SD) for resting blood flow during the hypercapnia runs. Rows six and seven show corresponding maps of T-statistic (β_0 divided by GLM residual SE).

techniques. However, this is likely due to spatial variations in the tSNR. Inspection of the raw effect-size maps for this response reveals more homogeneous apparent flow responses throughout cortical GM (rows 3 and 4), particularly for the pCASL sequence (statistical inference is not possible with these maps, but they are a more direct reflection of the response amplitude). Maps of absolute Δ CBF (bottom two rows) exhibited similar patterns to the effect-size maps.

Visual Response Maps and ROIs

In spite of the differences observed between subjects and pulse sequences for CO₂ responses, both PASL and pCASL resulted in similar maps of visual activation, demonstrating good sensitivity and specificity as indicated in the statistical maps shown in the top two rows of Fig. 4. These maps allowed calculation of visual ROIs for use in the other quantitative analyses shown below. The ROIs thus computed were of generally comparable extent and position for both methods.

Temporal SNR of Baseline CBF

Group average tSNR for GM and VC is shown as bar graphs in Fig. 5a. The tSNR values computed for

pCASL were generally higher than those found for PASL, a difference that achieved statistical significance ($P < 0.01$) in the GM ROI. Respective tSNR values for PASL and pCASL in GM were 1.9 ± 0.1 and 2.4 ± 0.2 ; those in VC were 2.4 ± 0.1 and 2.7 ± 0.2 .

In spite of the higher tSNR of pCASL (Fig. 5a), the increased imaging rate of PASL resulted in equivalent statistical power in the two types of image series, leading to similar detection rates for resting blood flow in GM voxels, as shown in Fig. 5b. The respective percent detection rates for resting CBF in GM voxels with PASL and pCASL were 93 ± 2 and 95 ± 1 . Resting CBF detection rates within the VC mask (ie, the fraction of voxels within the VC that exhibited baseline flow signal significantly different from 0) were 98.1 ± 0.8 (PASL) and 97.5 ± 0.9 (pCASL). Average T-values for resting CBF in GM were 23 ± 2 (PASL) and 25 ± 2 (pCASL); T-values in VC were 29 ± 2 (PASL) and 26 ± 3 (pCASL).

Functional Flow Changes

The ability to impose targeted changes in $P_{ET}CO_2$ allowed us a high degree of reproducibility of the stimulus. Nonetheless, while individual results

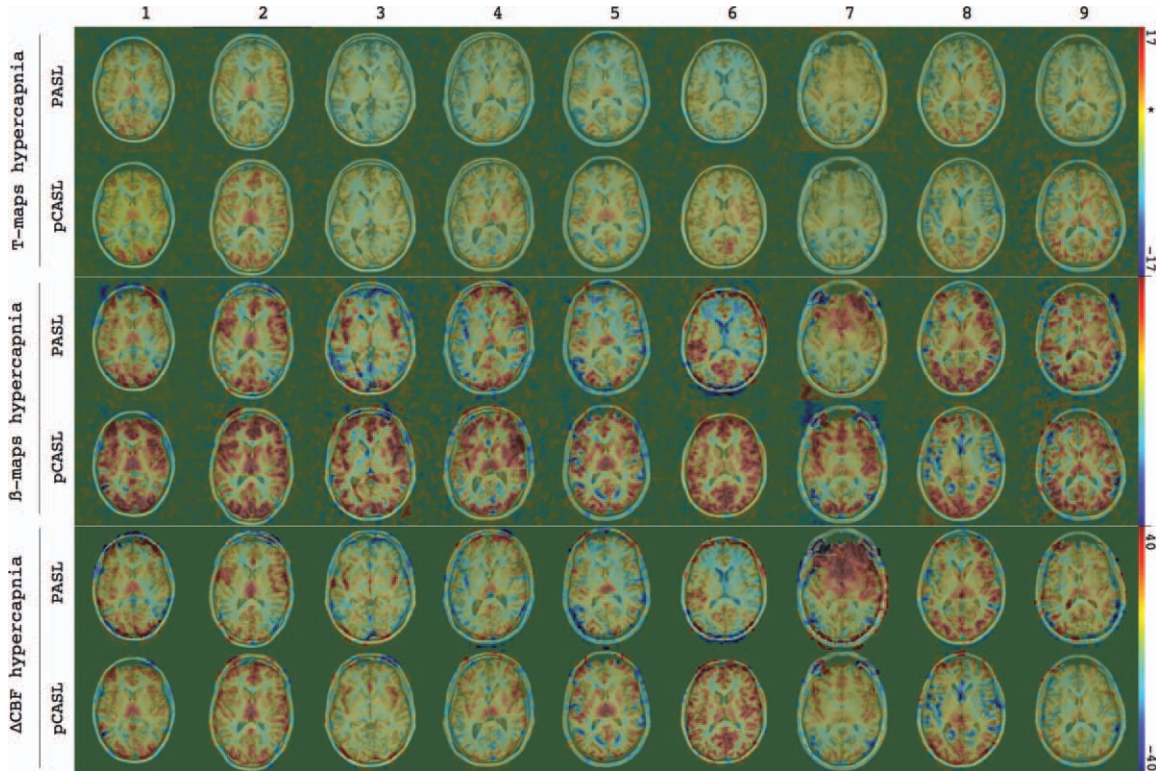


Figure 3. Hypercapnia response maps. Rows one and two show maps of T statistic for the CBF response to hypercapnia as measured using PASL and pCASL, respectively. The color mapping for T statistic values has been adjusted so that the transition from yellow to orange, indicated by the star, corresponds to $P < 0.001$ (corrected). Rows three and four show maps of the GLM effect sizes of the CBF response. Rows five and six show the size of the flow change, given in mL/min/100g.

demonstrated control within a tolerance of ± 2 mmHg in different individuals and scans, the range of CVR measures in GM was much larger in PASL than in pCASL ([0.7–6.1] vs. [3.0–5.2] $\Delta\%/mmHg$, respectively).

Figure 6 shows percent flow increases in response to hypercapnia and visual stimulation obtained using the two ASL sequences in different ROIs (converted, in the case of hypercapnia, to a CVR index by dividing by the increase in P_{ETCO_2}). Both methods show

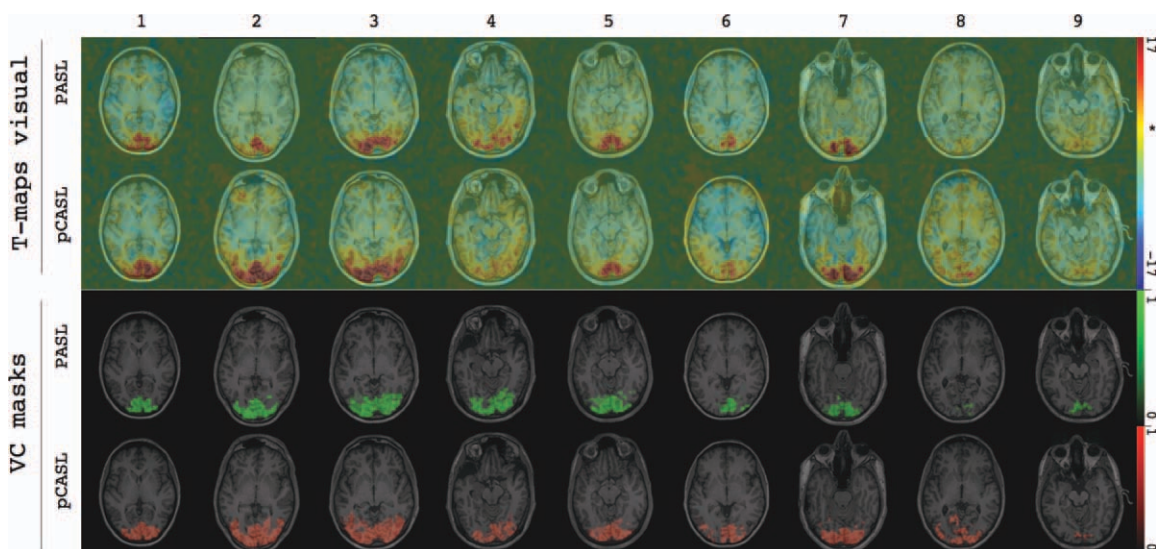


Figure 4. Visual response maps and VC masks. Rows one and two show maps of T statistic for the CBF response to visual stimulation for PASL and pCASL data, respectively. The color mapping for T statistic values has been adjusted so that the transition from yellow to orange, indicated by the star, corresponds to $P < 0.001$ (corrected). Rows three and four show ROIs encompassing VC in the different subjects, based on the visual activation data from the respective ASL sequences (green for PASL, red for pCASL).

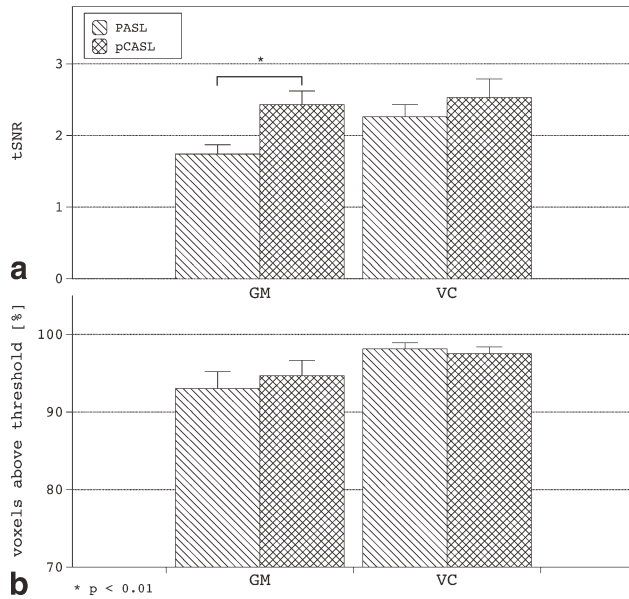


Figure 5. Temporal SNR and sensitivity for baseline flow. **a:** tSNR for baseline CBF (mean \pm SE) computed in GM and VC. **b:** Percent of GM and VC voxels with statistically significant baseline flow signal.

comparable values for the visually evoked flow increases, with the exception of values averaged over the union VC ROI, which were significantly different. For the hypercapnic responses, PASL resulted in apparent CVR values that were systematically and significantly ($P < 0.05$) smaller than those measured using pCASL. This was observed using ROIs covering both all GM and VC. Comparisons were repeated using different criteria for the VC ROIs (ie, technique-

specific, intersection, and union VC ROIs) and these were found to provide consistent results in all cases.

Results for individual subjects and group averages are summarized in Table 1.

Figure 7a shows the average T-values for the hypercapnic response in GM and VC, while Fig. 7b shows the corresponding detection rates (the two measures convey related but not identical information about the distribution and extent of the apparent response). The average T-value provided by pCASL for CO₂ response in GM was greater ($P < 0.03$) than that measured with PASL. The PASL average T-value was 2.0 ± 0.3 , while that obtained with pCASL was 2.9 ± 0.4 . PASL and pCASL average T-values of CO₂ response in VC were: 3.9 ± 0.6 and 5.2 ± 0.6 . The difference between the latter values was only marginally significant ($P < 0.08$) with both values higher ($P < 0.05$ and $P < 0.005$) than the corresponding T-values computed in GM. The pCASL sequence detected GM responses to hypercapnia at a significantly higher rate ($27 \pm 5\%$) than PASL ($16 \pm 3\%$ detection). In VC the corresponding detection rates for the CO₂ response were 56 ± 7 and 42 ± 9 .

Visual responses measured by PASL and pCASL in V1 were similar. Although the extent and amplitude of the pCASL response tended to be larger, the differences did not achieve statistical significance. The visual detection counts for PASL and pCASL, respectively, were 290 ± 60 and 400 ± 100 voxels (counts instead of percentage rates are used here because no independent segmentation of VC was available as in the case of GM). The visually evoked percent change in CBF measured by PASL was $75 \pm 5\%$, while that measured by pCASL was $81 \pm 4\%$. Average T-values in V1 for the visual activation were 9.6 ± 0.8 for PASL

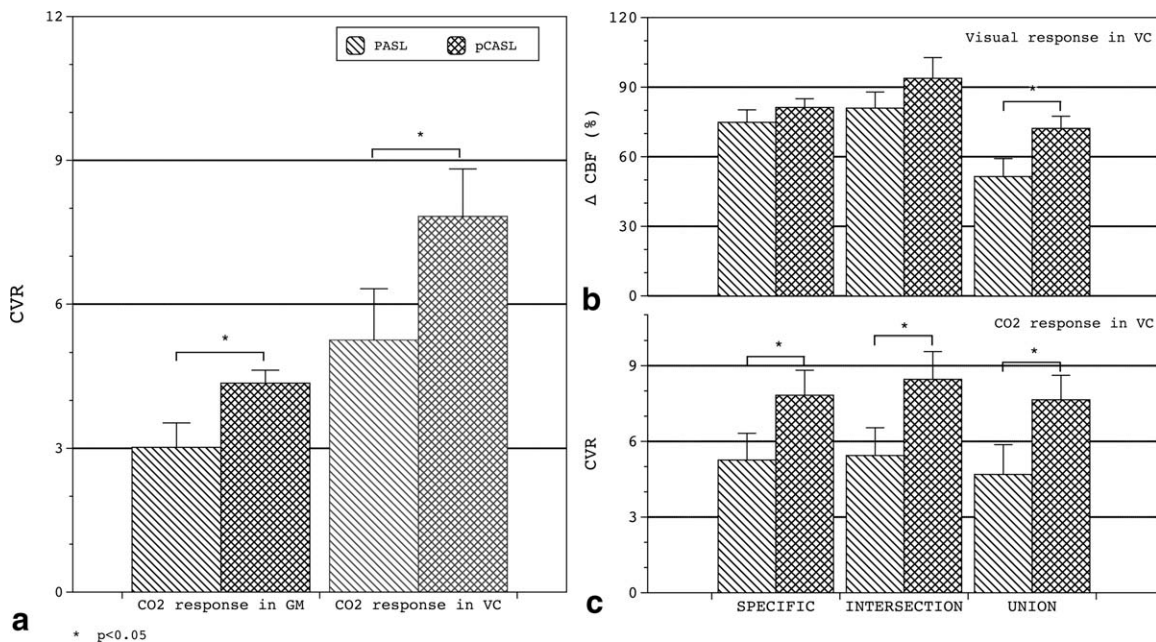


Figure 6. CBF responses to hypercapnia and visual stimulation. **a:** CVR to hypercapnia measured in GM and VC ROIs. **b:** Δ %CBF values for visual stimulation in VC. **c:** CVR measured in VC as delineated using alternate ROI selection criteria: 1) technique-specific (this approach is used in A); 2) intersection; and 3) union.

Table 1
Individual Baseline Flow and Responses

	$\Delta P_{ET}CO_2$ (mmHg)	Hypercapnia in GM			Hypercapnia in VC			Visual response in VC
		Baseline (mL/min/ 100g)	Response ($\Delta\%$ CBF)	CVR ($\Delta\%$ CBF/ mmHg)	Baseline (mL/min/ 100g)	Response ($\Delta\%$ CBF)	CVR ($\Delta\%$ CBF/ mmHg)	Response ($\Delta\%$ CBF)
PASL								
subject 1	3.3	56.3	17.7	3.3	63.6	26.5	5.0	53.2
subject 2	5.4	34.2	15.5	2.9	59.3	21.8	4.0	70.2
subject 3	4.0	62.0	5.1	1.3	58.6	5.1	1.3	81.1
subject 4	3.7	52.6	15.7	2.8	48.2	29.6	5.2	92.2
subject 5	4.0	52.8	16.3	4.1	47.1	35.0	8.8	61.0
subject 6	4.7	73.4	5.8	1.2	93.7	10.5	2.2	77.2
subject 7	4.7	52.9	3.2	0.7	67.1	11.8	2.5	89.8
subject 8	5.2	49.6	25.8	5.0	52.7	48.3	9.3	94.9
subject 9	3.8	39.4	23.2	6.1	44.6	35.5	9.4	53.9
mean \pm SE	4.8 \pm 0.2	56 \pm 3	14 \pm 3	3.0 \pm 0.6	59 \pm 5	25 \pm 5	5 \pm 1	75 \pm 5
pCASL								
subject 1	5.4	50.6	27.4	5.1	49.2	46.0	8.5	74.3
subject 2	5.6	66.8	27.0	4.8	53.1	36.2	6.5	76.5
subject 3	3.9	49.9	16.7	4.3	34.1	26.7	6.8	96.6
subject 4	5.5	54.9	19.4	3.5	49.1	28.2	5.1	68.4
subject 5	4.2	56.2	21.3	5.2	39.0	49.7	11.8	74.9
subject 6	5.1	81.2	15.5	3.0	85.7	12.6	2.5	60.0
subject 7	4.2	57.0	17.4	4.1	43.5	40.4	9.6	83.6
subject 8	4.1	46.0	18.8	4.6	41.2	42.9	10.5	99.6
subject 9	3.7	43.5	18.1	4.9	32.8	33.1	9.5	88.5
mean \pm SE	4.6 \pm 0.3	56 \pm 4	20 \pm 1	4.4 \pm 0.2	48 \pm 5	35 \pm 4	8 \pm 1	81 \pm 4

$\Delta P_{ET}CO_2$ is the increase in end-tidal CO_2 during the hypercapnia scan. Columns 2 and 5 show baseline flow values measured in gray matter (GM) and in the visual cortex (VC) ROIs, respectively. ROI-averaged percent changes, ie, flow responses, are shown in columns 3, 6, and 8. Columns 4 and 7 show cerebrovascular reactivity (CVR) values, computed as the flow response per mmHg of $\Delta P_{ET}CO_2$.

and 9.7 ± 0.9 for pCASL. ROI average values quoted here are for technique-specific VC ROIs.

While the visually evoked flow response may be stronger than the response to a mild hypercapnic stimulus, the response is local, limited to the VC. The VC, although extensive, is just a fraction of the total volume of the brain, and so is the brain's total flow increase with respect to the local flow increase. We found that the GM averaged flow percent change during visual stimulations were $5 \pm 2\%$ and $7 \pm 3\%$ for PASL and pCASL, respectively. These two figures correspond to $\approx 40\%$ of the flow changes in GM as computed to the hypercapnic stimulus.

DISCUSSION

In this study we compared the performance of pulsed and pseudocontinuous ASL sequences for measuring global CBF responses elicited by mild hypercapnia. We also compared results obtained for resting cerebral blood flow and focal visual stimulation. A number of differences were noted, which may be due to the different temporal characteristics of the two labeling approaches.

Early implementations of the QUIPSS II method (22) used an interval TI1 between the inversion and the onset of saturation pulses of 700 msec, with a label slab thickness of 100 mm (the limited thickness probably due to use of a transmit-receive head coil for inversion). This initial report showed that, at global

CBF rates observed during rest or during moderate focal activation such as that produced by finger

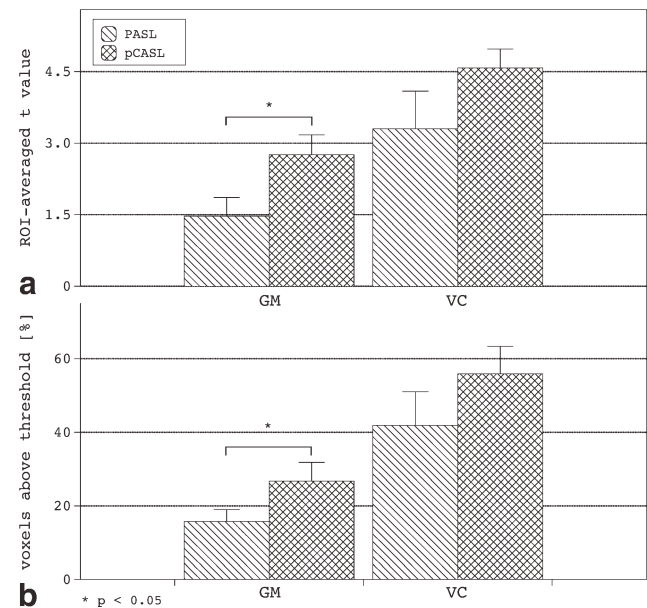


Figure 7. Average T-values and detection power for hypercapnic responses. **a:** Average T statistic values (mean \pm SE) for the CBF response to hypercapnia measured in GM and VC. **b:** Percent of GM and VC voxels showing statistically significant response to the stimulus.

tapping, the trailing edge of a 100-mm label bolus would take longer than 700 msec to exit the initial tagging region (meaning that the QUIPSSII saturation would control the tag duration). However, during global flow increases, which are known to have a large impact on the flow velocity in the major arteries feeding the brain (14), it is quite possible that the trailing edge of the label bolus will clear the tag region prior to T1, rendering any QUIPSS II saturation pulses ineffective and creating a situation that may underestimate flow. This concern can be mitigated to some extent by using a thicker label slab (ie, 150–200 mm) as done in the present study, but in general there may always be some level of global flow above which the control of label duration by spatially selective saturation becomes ineffective.

In CASL, the control over the label duration is implicit, thus relieving the latter concern. Such techniques also offer an increase in the tSNR of individual flow subtraction images, although the imaging rate is typically somewhat lower; and a reduction in variability due to pulsatile changes in flow velocity during the cardiac cycle (29). A potential confound in CASL methods (including pCASL) is that the labeling efficiency may suffer from field inhomogeneities, and vary if there are large changes in arterial flow. However, because of the use of a short gap (360 μ s) between RF pulses in our pCASL implementation, the label efficiency is relatively insensitive to potential field inhomogeneity effects at the labeling location. Dai et al (30) showed that efficiency is at least 80% as long as field inhomogeneity is within 3 ppm at 3T. This value was estimated based on theoretical calculations by Wu et al (8) in which the flow velocity was varied from 20 to 80 cm/s, and further verified experimentally in a recent study (16) using phase-contrast MRI as the reference.

Our results indicate that the intrinsic the per-image tSNR of the continuous method remains higher (Fig. 2, 4th and 5th rows; Fig. 5a). The increased imaging rate of PASL, however, compensates for this, as shown by the maps of T-value (Fig. 2, last two rows) and the number of voxels after thresholding of T-maps (Fig. 5b). Indeed, PASL and pCASL provide maps (Fig. 2, 2nd and 3rd rows) and absolute values of baseline flow that are virtually indistinguishable (Table 1), indicating that both methods are good candidates for imaging and quantifying resting CBF in healthy volunteers. Nevertheless, different results might be obtained in the case of abnormally slow flow rates, as these could exacerbate T1 label decay, which is more prevalent in pulsed methods.

The most notable differences between the two ASL methods were found in the depiction of the hypercapnia responses. Inspection of the T-maps for the CO₂ manipulation (Fig. 3, first two rows) reveals that the anticipated pattern of GM response is poorly demonstrated for most subjects in both PASL and pCASL. This is surprising, since BOLD data during comparable manipulations consistently indicates a very strong hemodynamic response throughout GM (4). However, the effect-size maps give a more direct indication of the response amplitude (middle two rows) than the T-

maps, in which there is a division by the residual standard error. It is likely that the spatial patterns seen in the T-maps are largely driven by the spatial patterns of noise, which tend to obscure the globally uniform GM flow response. When the effect-size maps are considered, it is apparent that pCASL provides a more reliable depiction of the global GM response (note lack of PASL response in large areas of cortical GM in subjects 2, 3, 4, and 7). Although the effect-size maps provide a qualitative depiction of the response pattern, they are closely related to maps of absolute change, which can be computed using the approach described above for resting CBF. Quantitative maps of Δ CBF (bottom two rows) are computed in this way and the response measured by pCASL appears to demonstrate a more uniform depiction of GM flow increases.

The mean T-value for hypercapnic response within the GM and visual ROI masks was consistently higher for pCASL, achieving statistical significance for the average over the GM mask (Fig. 7a). This corresponded with increased voxel detection rates by pCASL for hypercapnia, as shown in Fig. 7b. This latter bar graph shows the percentage of voxels within the GM and VC masks in which the ASL T-values for hypercapnic response exceeded a threshold corresponding to $P \leq 0.05$ (corrected). Since it can be assumed that, in reality, all GM voxels underwent increased blood flow in the healthy volunteers imaged in this study, the low detection rates indicate that thresholded T-maps of hypercapnic CBF response are likely to be unreliable for the assessment of CVR, regardless of ASL technique.

Figure 6 shows estimated CVR values as measured with PASL and pCASL. The estimated CVR values provided by pCASL are significantly higher than those measured with PASL in both regions GM and VC. This difference was apparent regardless of the ROI prescription method used (technique-specific, intersection, or union). In contrast, the visually evoked responses were not significantly different, except when averaged over the union of activated areas detected by both methods. This is probably due to both the large amplitude of the visually evoked response and the fact that pulsed ASL tag dynamics are less affected by focal than by global flow changes. It should be noted that, in spite of the large peak amplitude of the visual flow response, when averaged over all GM it represents a substantially smaller increase in whole-brain blood flow ($7 \pm 3\%$ via pCASL) than hypercapnia (20 ± 1). The difference found for the union ROI can be explained by the fact that pCASL tended to yield visually evoked changes over a more extensive region than did PASL.

Although similar responses were observed for focal flow increases, our results show a systematic reduction in the apparent CO₂-induced flow increase measured with PASL relative to values obtained with pCASL. The demonstration that PASL and pCASL yield virtually indistinguishable values for resting CBF, as well as for visually evoked flow responses, reinforces our suspicion that global physiological manipulations like mild hypercapnia pose a special challenge for PASL methods. Our results suggest that

typical implementations of PASL may fail to control tag timing at high CBF rates, thereby underestimating CBF responses.

In conclusion, the use of pCASL instead of PASL may help improve the sensitivity and accuracy of MRI measurements relying on global manipulation such as measurements of CVR and CMRO₂.

The lack of a “gold standard” measure of CVR prevents us from ruling out the possibility that pCASL is also affected by sources of systematic error during hypercapnia, such as reductions in labeling efficiency as postulated by Aslan et al (16) (who postulated a 36% underestimation of the CBF change during a 9 mmHg increase in P_{ET}CO₂, which could imply an underestimation of CBF change in our 5 mmHg manipulation by up to 20%). Further study using methods such as phase-contrast flow quantification is clearly warranted. Another promising avenue of investigation is the use of pulsed or continuous ASL methods with variable delay times (31), which allow measurement of the tag inflow curve and, by fitting with kinetic models, quantitative estimation of CBF. These may help refining and validating single-subtraction versions of ASL techniques.

ACKNOWLEDGMENT

We thank Carolyn Hurst and André Cyr for help with data acquisition. This work was supported by the Canadian Institutes for Health Research (MOP 84378, Banting and Best Scholarship held by CJG), the Canadian Foundation for Innovation (Leaders Opportunity Fund 17380), and the Ministère du développement économique, de l'innovation et de l'exportation (PSR- SIIRI-239).

REFERENCES

- Kety SS, Schmidt CF. The effects of altered arterial tensions of carbon dioxide and oxygen on cerebral blood flow and cerebral oxygen consumption of normal young men. *J Clin Invest* 1948; 27:484–492.
- Ellingsen I, Hauge A, Nicolaysen G, Thoresen M, Walløe L. Changes in human cerebral blood flow due to step changes in PAO₂ and PACO₂. *Acta Physiol Scand* 1987;129:157–163.
- Kastrup A, Krüger G, Glover GH, Moseley ME. Assessment of cerebral oxidative metabolism with breath holding and fMRI. *Magn Reson Med* 1999;42:608–611.
- Mark CI, Slessarev M, Ito S, Han JS, Fisher JA, Pike GB. Precise control of end-tidal carbon dioxide and oxygen improves BOLD and ASL cerebrovascular reactivity measures. *Magn Reson Med* 2010;64:749–756
- Hoge RD, Atkinson J, Gill B, Crelier GR, Marrett S, Pike GB. Linear coupling between cerebral blood flow and oxygen consumption in activated human cortex. *Proc Natl Acad Sci U S A* 1999; 96:9403–9408.
- Ances BM, Liang C, Leontiev O, et al. Effects of aging on cerebral blood flow, oxygen metabolism, and blood oxygenation level dependent responses to visual stimulation. *Hum Brain Mapp* 2009; 30:1120–1132.
- Detre JA, Leigh JS, Williams DS, Koretsky AP. Perfusion imaging. *Magn Reson Med* 1992;23:37–45.
- Wu W-C, Fernández-Seara MA, Detre JA, Wehrli FW, Wang J. A theoretical and experimental investigation of the tagging efficiency of pseudocontinuous arterial spin labeling. *Magn Reson Med* 2007;58:1020–1027.
- Alsop DC, Detre JA. Reduced transit-time sensitivity in noninvasive magnetic resonance imaging of human cerebral blood flow. *J Cereb Blood Flow Metab* 1996;16:1236–1249.
- Mildner T, Möller HE, Driesel W, Norris DG, Trampel R. Continuous arterial spin labeling at the human common carotid artery: the influence of transit times. *NMR Biomed* 2005;18:19–23.
- Yang Y, Engelen W, Xu S, Gu H, Silbersweig DA, Stern E. Transit time, trailing time, and cerebral blood flow during brain activation: measurement using multislice, pulsed spin-labeling perfusion imaging. *Magn Reson Med* 2000;44:680–685.
- Wong EC, Buxton RB, Frank LR. Quantitative imaging of perfusion using a single subtraction (QUIPSS and QUIPSS II). *Magn Reson Med* 1998;39:702–708.
- Luh WM, Wong EC, Bandettini P, Hyde JS. QUIPSS II with thin-slice T1 periodic saturation: a method for improving accuracy of quantitative perfusion imaging using pulsed arterial spin labeling. *Magn Reson Med* 1999;41:1246–1254.
- Markwalder TM, Grolimund P, Seiler RW, Roth F, Aaslid R. Dependency of blood flow velocity in the middle cerebral artery on end-tidal carbon dioxide partial pressure—a transcranial ultrasound Doppler study. *J Cereb Blood Flow Metab* 1984;4:368–372.
- Pohmann R, Budde J, Auerbach EJ, Adriany G, Ugurbil K. Theoretical and experimental evaluation of continuous arterial spin labeling techniques. *Magn Reson Med* 2010;63:438–446.
- Aslan S, Xu F, Wang PL, et al. Estimation of labeling efficiency in pseudocontinuous arterial spin labeling. *Magn Reson Med* 2010; 63:765–771.
- Wong EC, Buxton RB, Frank LR. A theoretical and experimental comparison of continuous and pulsed arterial spin labeling techniques for quantitative perfusion imaging. *Magn Reson Med* 1998;40:348–355.
- Wang J, Alsop DC, Li L, et al. Comparison of quantitative perfusion imaging using arterial spin labeling at 1.5 and 4.0 Tesla. *Magn Reson Med* 2002;48:242–254.
- Chen Y, Wang DJJ, Detre JA. Test-retest reliability of arterial spin labeling with common labeling strategies. *J Magn Reson Imaging* 2011;33:940–949.
- Slessarev M, Han JS, Mardimae A, et al. Prospective targeting and control of end-tidal CO₂ and O₂ concentrations. *J Physiol (Lond)* 2007;581:1207–1219.
- Prisman E, Slessarev M, Han J, et al. Comparison of the effects of independently-controlled end-tidal PCO₂ and PO₂ on blood oxygen level-dependent (BOLD) MRI. *J Magn Reson Imaging* 2008;27:185–191.
- Wong EC, Buxton RB, Frank LR. Implementation of quantitative perfusion imaging techniques for functional brain mapping using pulsed arterial spin labeling. *NMR Biomed* 1997;10:237–249.
- Griswold MA, Jakob PM, Heidemann RM, et al. Generalized auto-calibrating partially parallel acquisitions (GRAPPA). *Magn Reson Med* 2002;47:1202–1210.
- Cox RW, Jesmanowicz A. Real-time 3D image registration for functional MRI. *Magn Reson Imaging* 1999;42:1014–1018.
- Glover GH. Deconvolution of impulse response in event-related BOLD fMRI. *NeuroImage* 1999;9:416–429.
- Worsley KJ, Liao CH, Aston J, et al. A general statistical analysis for fMRI data. *NeuroImage* 2002;15:1–15.
- Wang J, Aguirre GK, Kimberg DY, Roc AC, Li L, Detre JA. Arterial spin labeling perfusion fMRI with very low task frequency. *Magn Reson Med* 2003;49:796–802.
- Wang J, Alsop DC, Song HK, et al. Arterial transit time imaging with flow encoding arterial spin tagging (FEAST). *Magn Reson Med* 2003;50:599–607.
- Wu W-C, Mazaheri Y, Wong EC. The effects of flow dispersion and cardiac pulsation in arterial spin labeling. *IEEE Trans Med Imaging* 2007;26:84–92.
- Dai W, Garcia DM, de Bazelaire C, Alsop DC. Continuous flow-driven inversion for arterial spin labeling using pulsed radio frequency and gradient fields. *Magn Reson Med* 2008;60:1488–1497.
- Ho Y-CL, Petersen ET, Zimine I, Golay X. Similarities and differences in arterial responses to hypercapnia and visual stimulation. *J Cereb Blood Flow Metab* 2011;31:560–571.